Theoretical x-ray absorption Debye-Waller factors

Fernando D. Vila and J. J. Rehr
Department of Physics, University of Washington, Seattle, Washington 98195, USA

H. H. Rossner and H. J. Krappe
Hahn-Meitner-Institut Berlin, Glienicker Strasse 100, D-14109 Berlin, Germany

(Received 14 February 2007; revised manuscript received 10 April 2007; published 5 July 2007)

An approach is presented for theoretical calculations of the Debye-Waller factors in x-ray absorption and related spectra. These damping factors are represented in terms of the cumulant expansion up to third order. They account respectively for the net thermal expansion $\sigma^{(1)}(T)$, the mean-square relative displacements $\sigma^2(T)$, and the asymmetry of the pair distribution function $\sigma^{(3)}(T)$. Similarly, we obtain Debye-Waller factors for x-ray and neutron scattering in terms of the mean-square vibrational amplitudes $u^2(T)$. Our method is based on density functional theory calculations of the dynamical matrix, together with an efficient Lanczos algorithm for projected phonon spectra within the quasiharmonic approximation. Because of the anharmonicity in the interatomic forces, the results are highly sensitive to variations in the equilibrium lattice constants, and hence to the choice of exchange-correlation potential. In order to treat this sensitivity, we introduce two prescriptions: one based on the local density approximation, and a second based on a modified generalized gradient approximation. Illustrative results for the leading cumulants are presented for several materials and compared with experiment and with correlated Einstein and Debye models. We also obtain Born-von Karman parameters and corrections due to perpendicular vibrations.

DOI: 10.1103/PhysRevB.76.014301 PACS number(s): 07.05.Tp, 61.10.Ht, 87.64.Fb

I. INTRODUCTION

Thermal vibrations and disorder in x-ray absorption spectra (XAS) and related spectroscopies give rise to Debye-Waller (DW) factors varying as $\exp[-W(T)]$, where $W(T) \approx 2k^2\sigma^2(T)$ and $\sigma^2(T)$ is the mean square relative displacement (MSRD) of a given multiple-scattering (MS) path.[1] These Debye-Waller factors damp the spectra with respect to increasing temperature T and wave number k (or energy), and account for the observation that the x-ray absorption fine structure (XAFS), "melts" with increasing temperature.[2] Identical DW factors apply to related spectroscopies which can be described by a multiple-scattering path expansion, such as extended electron energy loss fine structure (EXELFS). The XAFS DW factor is analogous to that for x-ray and neutron diffraction or the Mößbauer effect, where $W(T)=(1/2)k^2u^2(T)$. The difference is that the XAFS DW factor refers to correlated averages over relative displacements, e.g., $\sigma^2=\langle[(\mathbf{u}_R-\mathbf{u}_0)\cdot\hat{\mathbf{R}}]^2\rangle$ for the MSRD, while that for x-ray and neutron diffraction refers to the mean-square displacements $u^2(T)=\langle(\mathbf{u}\cdot\hat{\mathbf{R}})^2\rangle$ of a given atom. Due to their exponential damping, accurate DW factors are crucial to a quantitative treatment of x-ray absorption spectra. Consequently, the lack of precise DW factors has been one of the biggest limitations to accurate structure determinations (e.g., coordination number and interatomic distances) from XAFS experiment.

Because of the difficulty of calculating the vibrational distribution function from first principles, XAFS DW factors have, heretofore, been fitted to experimental data or estimated semiempirically, e.g., from correlated Einstein and Debye models.[3,4] However, these approaches are unsatisfactory for several reasons. First, there are typically many more independent DW factors in the XAFS MS path expansion than can be fit reliably to the available data. Second, the semiempirical models require separate fits to appropriate Debye or Einstein temperatures for each multiple-scattering path. And third, these models typically ignore anisotropic contributions, and hence do not capture the detailed structure of the phonon spectra and associated DW factors.

To address these problems, we introduce here first principles procedures for calculations of the Debye-Waller factors in XAS and related spectra. Our approach is based on density functional theory (DFT) calculations of the dynamical matrix, together with an efficient Lanczos algorithm for the projected phonon spectra.[5,6] DFT calculations of crystallographic Debye-Waller factors and other thermodynamic quantities have been carried out previously using modern electronic structure codes,[7–9] and our work here builds on these developments, with particular emphasis on applications to XAS.

Due to intrinsic anharmonicity in the interatomic forces, the behavior of the DW factors is extremely sensitive to the equilibrium lattice constant a. For example, we find that σ^2 varies roughly as $a^{6\gamma}$, where $\gamma=-d\ln\bar{\omega}/d\ln V$ is the mean Grüneisen parameter which is typically about 2 for fcc metals, and $\bar{\omega}$ refers to the mean phonon frequency. Consequently σ^2 is also very sensitive to the choice of the exchange-correlation potential in the DFT, since a 1% error in lattice constant yields an error of $6\gamma\approx 12\%$ in σ^2. As a result, relatively small errors in the lattice constant predicted by the local density approximation (LDA) which tends to overbind, or the generalized gradient approximation (GGA) which tends to underbind, become greatly magnified[10] in DW calculations.

In order to treat this sensitivity and stabilize the calculations we have developed two prescriptions for *ab initio* calculations of DW factors based on DFT calculations with (I) the conventional LDA and (II) a modified-GGA (termed

hGGA) described below. For comparison we also present selected results with a conventional GGA, with the correlated Einstein and Debye models, and with an empirical model based on the Born–von Karman parameters obtained from fits to phonon spectra. Detailed results are presented for a number of fcc and diamond structures.

II. FORMALISM

A. Cumulants

In this section we outline the formalism used in our approach. Physically, the DW factors in XAS and related spectra (EXELFS, x-ray Raman spectra, etc.) arise from a thermal and configurational average of the spectra $\langle \mu(E) \rangle$ over the pair (or MS path length) distribution function, where $\mu(E)$ is the x-ray absorption coefficient in the absence of disorder. The effects of disorder and vibrations are additive, but since the factors due to configurational disorder are dependent on sample history and preparation, in this paper we focus only on the thermal contribution. The effect of the vibrations on the normalized x-ray absorption fine structure $\chi(k)=(\mu-\mu_0)/\mu_0$ is dominated by the average over the oscillatory behavior $\chi_R(k) \propto \sin(2kR+\Phi)$ of each path in the multiple-scattering (MS) path expansion. Thus these DW factors depend only on the path-length distribution function, and hence are the same for any spectroscopy which can be described by the MS path expansion. If the disorder is not too large the average can be expressed in terms of the cumulant expansion[1,11]

$$\langle e^{i2kr} \rangle \equiv e^{2ikR_0} e^{-W(T)}, \tag{1}$$

$$W(T) = -\sum_{n=1}^{\infty} \frac{(2ik)^n}{n!} \sigma^{(n)}(T), \tag{2}$$

where r is the instantaneous bond length or relative displacement, R_0 the equilibrium length in the absence of vibrations, and $\sigma^{(n)}(T)$ the nth cumulant average. For multiple-scattering paths, this length refers to half the total MS path length. The dominant effect on XAFS amplitudes comes from the leading exponential decay factor $W(T) \approx 2k^2\sigma^2(T)$. The expressions for the cumulants simplify when expressed with respect to the mean,[1] and hence σ^2 is given by the MSRD

$$\sigma^{(2)} = \langle (r-\bar{r})^2 \rangle \equiv \sigma^2(T). \tag{3}$$

The imaginary terms in $W(T)$ contributes to the XAFS phase. The leading contribution is the thermal expansion which comes from the first cumulant $\sigma^{(1)}(T)$

$$\sigma^{(1)} = \langle r - R_0 \rangle. \tag{4}$$

Thus, the mean bond length between atoms at the origin and site R is $\langle r \rangle \equiv \bar{r} = R_0 + \sigma^{(1)}(T)$. Following the analysis of Fornasini *et al.*[12] it is convenient to express the instantaneous relative displacement vector in terms of displacements parallel and perpendicular to the bond $\mathbf{0}-\mathbf{R}$, i.e., $\Delta\mathbf{u} = \mathbf{u}_R - \mathbf{u}_0 = \Delta\mathbf{u}_\parallel + \Delta\mathbf{u}_\perp$. Then the first cumulant up to terms quadratic in the relative displacements is given by

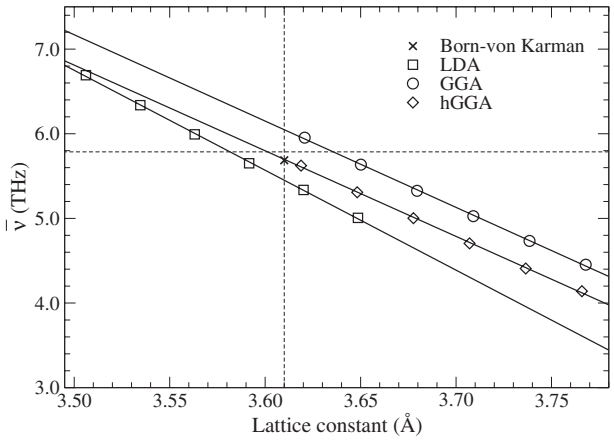

FIG. 1. Mean frequency $\bar{\nu}$ of the VDOS projected along the nearest-neighbor single scattering path of Cu, obtained from the first Lanczos iteration. The vertical line indicates the experimental lattice constant at 298 K while the horizontal line shows the Einstein frequency obtained from the experimentally determined DW factor. The Born-von Karman parameters for Cu at 298 K were taken from Ref. 13.

$$\sigma^{(1)} = \left\langle \Delta u_\parallel + \frac{\Delta u_\perp^2}{2R} \right\rangle \equiv \sigma_\parallel^{(1)} + \sigma_\perp^{(1)}. \tag{5}$$

The first term $\sigma_\parallel^{(1)}$ corresponds to the lattice expansion as measured in x-ray and neutron diffraction. Thus vibrations perpendicular to a given bond lead to an increase in the mean expansion observed in XAFS compared to that in crystallography

$$\sigma_\perp^{(1)} = \frac{\langle |\Delta\mathbf{u}_\perp|^2 \rangle}{2R_0} \equiv \frac{\sigma_\perp^2}{2R_0}. \tag{6}$$

We have found (see Appendix) that the mean square perpendicular displacement (MSPD) $\sigma_\perp^2$ and the MSRD σ^2 are are closely related and that $\sigma_\perp^2$ can be estimated from σ^2 using lattice dynamical models.

Next, the skew of the distribution, which is defined by the third cumulant $\sigma^{(3)}(T)$, contributes a negative phase shift, and hence the mean distance obtained in fits to XAFS experiment is typically shorter than that obtained from the first cumulant alone.[1] Here

$$\sigma^{(3)} = \langle (r-\bar{r})^3 \rangle. \tag{7}$$

As emphasized above, an accurate account of the effects of anharmonicity is key to a quantitative treatment of these DW factors over a broad range of temperatures. The effects of anharmonicity are illustrated in Fig. 1, which shows the strong variation in the mean phonon frequency $\bar{\nu}=\bar{\omega}/2\pi$ vs small variations in lattice constant as calculated using various models described below.

The thermal averages involved in the calculation of the cumulants can be expressed in terms of the projected vibrational density of states (VDOS) $\rho_R(\omega)$.[5,6,14] For example, the MSRD σ^2 for a given path R is given by the Debye integral

$$\sigma_R^2(T) = \frac{\hbar}{2\mu_R}\int_0^\infty \frac{1}{\omega}\coth\left(\frac{\beta\hbar\omega}{2}\right)\rho_R(\omega)d\omega, \tag{8}$$

where μ_R is the reduced mass associated with the path, $\beta = 1/k_BT$, and $\rho_R(\omega)$ is the vibrational density of states projected on R. In the following, the path index subscript R is suppressed unless needed for clarity.

The first cumulant $\sigma^{(1)}$ is generally path dependent and reflects the anharmonic behavior of a system. For monoatomic systems, this quantity is closely related to the net thermal expansion $\Delta a = a(T) - a_0$, which can be obtained by minimizing the vibrational free energy $F(a,T)$. Within the quasiharmonic approximation, $F(a,T)$ is given by a sum over the internal energy $E(a)$ and the vibrational free energy per atom

$$F(a,T) = E(a) + 3k_BT\int_0^\infty d\omega \ln\left[2\sinh\left(\frac{\beta\hbar\omega}{2}\right)\right]\rho_a(\omega), \tag{9}$$

where T is the temperature, $\rho_a(\omega)$ is the total VDOS, and we have assumed cubic symmetry for simplicity.

Finally in comparisons with experiment, it is important to recognize that the the position-dependent XAFS amplitude factors $\exp(-2R/\lambda)/R^2$, where λ is the EXAFS mean-free-path, give rise to an effective radial distribution function[12] $\tilde{g}(R) = g(R)\exp(-2R/\lambda)/R^2$ for the cumulant expansion which is slightly modified from the *real* radial distribution function $g(R)$. As a result the apparent thermal expansion observed in XAFS is slightly shifted from $\sigma^{(1)}$ by the quantity

$$\Delta\sigma^{(1)} = -\frac{2}{R}\left(1 + \frac{R}{\lambda}\right)\sigma^2. \tag{10}$$

This correction is often taken into account in XAFS analysis routines, and is included in the experimental results discussed here.[12] Note also that the contributions $\sigma_\perp^{(1)}$ in Eq. (6) and $\Delta\sigma^{(1)}$ in Eq. (10) are both of the same order of magnitude and partially cancel.

B. Lanczos algorithm

The VDOS $\rho_R(\omega)$ has often been approximated using Einstein or Debye models with empirical Einstein or Debye temperatures. Although these models are quite useful, especially for isotropic systems such as metals without highly directional bonds, their limitations are well known.[14,15] To overcome some of these limitations Poiarkova and Rehr[5,14] proposed a method in which the VDOS is calculated from the imaginary part of the lattice dynamical Green's function

$$\rho_R(\omega) = -\frac{2\omega}{\pi}\,\mathrm{Im}\left\langle 0\left|\frac{1}{\omega^2 - \mathbf{D} + i\epsilon}\right|0\right\rangle. \tag{11}$$

Here $|0\rangle$ is a Lanczos seed vector representing a normalized, mass-weighted initial displacement of the atoms along the multiple-scattering path R, and $\mathbf{D}$ is the dynamical matrix of force constants

$$D_{jl\alpha,j'l'\beta} = (M_jM_{j'})^{-1/2}\frac{\partial^2 E(a)}{\partial u_{jl\alpha}\partial u_{j'l'\beta}}, \tag{12}$$

where $u_{jl\alpha}$ is the $\alpha = \{x,y,z\}$ Cartesian displacement of atom j in unit cell l and M_j is the mass of atom j, and where $E(a)$ is the internal energy of the system evaluated at the lattice constant $a(T)$. Thus, our approach takes into account the main effects of anharmonicity in terms of force constants that depend parametrically on temperature.

Efficient calculations of the lattice dynamical Green's function can be accomplished using a continued fraction representation, with parameters obtained with the iterative Lanczos algorithm.[16] This yields a many-pole representation for the VDOS which is well suited for accurate spectral integrations. The first step in the Lanczos algorithm corresponds to a correlated Einstein model

$$\rho_R = \delta(\omega - \bar{\omega}), \tag{13}$$

with frequency $\bar{\omega}$ corresponding to the rms average over the projected phonon spectra $\rho(\omega)$ in Eq. (11),

$$\bar{\omega}^2 = \langle 0|\mathbf{D}(R)|0\rangle. \tag{14}$$

However, the most appropriate choice for an Einstein frequency depends on the physical quantity being calculated. For example, for the MSRD the Einstein frequency is determined by the inverse second moment of the VDOS rather than $\bar{\omega}$, as discussed below. Poiarkova *et al.* truncated the continued fraction at the second tier (i.e., second Lanczos iteration), which is usually adequate to converge the results to about 10%. Subsequently Krappe and Rossner[6] showed that at least six Lanczos iterations are required to achieve convergence to within 1%. Thus the Lanczos algorithm provides an efficient and accurate procedure for calculating MS path-dependent DW factors from Eq. (8).

The main difficulty in implementing the Lanczos algorithm lies in obtaining an accurate model for the dynamical matrix (or force constants) $\mathbf{D}$ for a given system. Although semiempirical estimates of interatomic force constants or Born–von Karman parameters are sometimes available, their temperature dependence limits their accuracy and generality. Similarly, simple models for the vibrational distribution function (e.g., Einstein and Debye) generally ignore anisotropic behavior. One of the main aims in this paper is to develop a first principles approach that allows us to calculate the force constants for various systems using DFT. In addition, we have extended the Lanczos algorithm described above to several other cases by generalizing the Lanczos seed state $|0\rangle$. This allows us to calculate the total vibrational density of states, the vibrational free energy, thermal expansion, the mean square atomic displacements $u^2(T)$ in crystallographic Debye-Waller factors.[17] In addition, we calculate $\sigma_\perp^2$, which yields the perpendicular motion contribution to the DW factor of Eq. (8), and estimates of the third cumulant. Representative results for the VDOS calculated by this method are illustrated in Fig. 2.

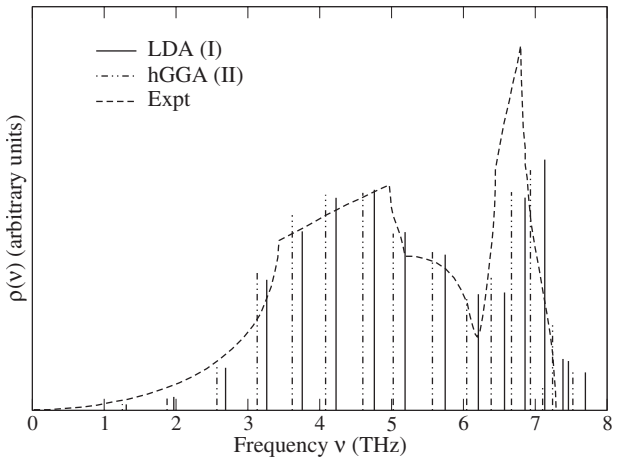

FIG. 2. Total vibrational density of states of Cu at 49 K from DFT calculations using the LDA with our prescription I; the hGGA (see text) with our prescription II; and from experiment (Ref. 12).

C. Correlated Einstein model

Although the cumulants other than the second are often negligible for small anharmonicity, their calculation using the apparatus of anharmonic lattice dynamics[18] is computationally demanding. On the other hand, it has been shown that these cumulants can be approximated to reasonable accuracy using a correlated anharmonic Einstein model for each MS path,[4,19] and this is the method adopted here. In this approach a correlated Einstein model is constructed for each MS path keeping only cubic anharmonicity, yielding an effective one-dimensional potential

$$V(x) = \frac{1}{2}k_0x^2 + k_3x^3, \tag{15}$$

where x is the net stretch in a given bond. The Einstein frequency ω_E within the quasi-harmonic approximation is then obtained from the relation (A4), i.e., $\mu\omega_E^2 = k = k_0 + 6k_3\bar{x}$. The construction of this Einstein model from the dynamical matrix **D** along with explicit examples is given in the Appendix. The relations between the cumulants for the Einstein model can then be used to obtain estimates for $\sigma^{(1)}$ and $\sigma^{(3)}$. For example, for the first cumulant one has

$$\sigma^{(1)}(T) = -\frac{3k_3}{k}\sigma^2(\bar{\omega},T) = -\eta\frac{3k_3}{k}\sigma^2(\omega_E,T), \tag{16}$$

where $\sigma^2(\bar{\omega},T)$ is the second cumulant of the Einstein model defined by Eq. (14) and $\eta = 1/\langle\omega^{-2}\rangle\bar{\omega}^2$ is defined so that $\sigma^2(\bar{\omega},T) \to \eta\sigma^2(\omega_E,T)$ at high temperatures. Thus the second relation on the right only apparently differs from that in Refs. 4 and 19. Analogous scaling factors appear in the single near-neighbor spring constant model derived by Maradudin and Flinn.[18]

III. DFT CALCULATIONS

A. Computational strategy

As noted above, one of the main aims of this paper is to calculate the force constants **D** within the quasiharmonic approximation using DFT and an appropriate choice of exchange-correlation functional. Due to the extreme sensitivity of the phonon spectra to the interatomic distances, as discussed above, the most important parameters entering the calculation of the dynamical matrix are the lattice constant and the geometry of the system. A typical effect of expansion is illustrated in Fig. 1, which shows the variation of the first moment of the VDOS (i.e., the average frequency $\bar{\nu}$) projected along the nearest-neighbor single-scattering path of Cu. For comparison Fig. 1 also shows $\bar{\nu}$ obtained with a model based on the Born–von Karman parameters at 298 K. As expected, when the system expands the vibrational frequencies are redshifted due to the weakening of the interatomic interactions. From the common slopes in Fig. 1, we see that all of the functionals have comparable Grüneisen parameters $\gamma \approx 2.2$ at the experimental lattice constant 3.61 Å, in accord with the experimental value[21] 2.0 ± 0.2. Note that although at a given lattice constant the GGA functional always produces a stiffer model than LDA, i.e., with higher mean frequencies, the results at the equilibrium GGA lattice constant tend to be softer than at the equilibrium LDA lattice constant. Moreover, when compared with the experimental value, the LDA and GGA functionals, respectively, underestimate and overestimate the mean frequency by about 5%. This translates into a 20–25 % error in the DW factors calculated with these methods. This margin of error is too large to make such calculations of significant value in quantitative EXAFS analysis. Based on the above considerations, we propose two alternative prescriptions to stabilize our DW factor calculations.

(I) Our first prescription is based on DFT calculations using the LDA exchange-correlation functional at the calculated equilibrium lattice constant $a(T)$ at a given temperature. Note, however, that the errors in the LDA estimates of the lattice constant are often larger than those obtained in fits to XAFS experiment.

(II) Our second prescription is based on DFT calculations using a modified GGA exchange-correlation functional termed hGGA (with half-LDA and half-GGA) at the experimentally determined lattice constant $a(T)$ at a given temperature. As described below, this functional is constructed on the assumption that the "true" functional lies somewhere between pure LDA and GGA. This second prescription may be useful when an estimate for the lattice constant is available, for example, in fits of XAFS data to experiment during which the interatomic distance is refined. Clearly, the use of experimental structural parameters limits prescription II, since it requires some knowledge of the crystal structure at each temperature of interest.

B. Exchange-correlation functionals

In the course of this work, we investigated a number of exchange-correlation functionals. Generally, the exchange-correlation functional is attractive and hence strongly affects the overall strength and curvature of the interatomic potential. On the other hand, it is well known that LDA functionals tend to overbind, yielding lattice constants smaller than experiment typically by about 1%. In contrast, GGA function-

als tend to underbind[10] by about the same amount. These errors are confirmed by our calculations, which show that for Cu the LDA yields a lattice constant of 3.57 Å at 0 K and 3.58 Å at 298 K, while the GGA yields 3.69 and 3.70 Å, respectively, experiment being 3.61 Å. Moreover, the effect of the functionals on the phonon structure is even larger. For example, Narasimhan and de Gironcoli[10] show that the thermal expansion is about 10% high with LDA and 10% low with GGA.

Although significant effort has been put into so-called meta-GGA functionals[23,24] that address these issues, they have not yet been widely implemented. Therefore, to be consistent with various results[10] and to preserve the advantages of the LDA and GGA functionals we have devised a modified functional termed hGGA which is a mixture of 50% LDA and 50% GGA, i.e., with a 50% reduction in both the additional exchange and correlation terms in the GGA. The motivation for the 50-50 mixture stems from the observation that the experimental values for many quantities are roughly bracketed by the LDA and GGA predictions. To simplify the development, we chose the closely related Perdew-Wang 92[25] (LDA) and Perdew-Burke-Ernzerhof[26] (GGA) functionals. For this case the equal parts mixing can be achieved with two simple changes: First, the κ parameter in the exchange energy term in PBE is reduced by half. This change preserves all the conditions on which PBE was founded, except the Lieb-Oxford bound. Second, the gradient contribution H to the correlation energy is also reduced by half. Similar modified functionals for solids have been proposed by Perdew *et al.*,[27] suggesting that modifications similar to the hGGA may be more generally applicable. Figure 1 shows the average frequency obtained with the hGGA functional and confirms that this yields the desired behavior.

C. Dynamical matrix

The key physical quantity needed in calculations of the Debye-Waller factors is the dynamical matrix **D**. With modern electronic structure codes this matrix of force constants can be calculated with sufficient accuracy from first principles both for periodic and molecular systems.[7–9] In this paper we restrict our attention to periodic systems which can be treated, for example, using the methodology implemented in the ABINIT code,[28] as described in detail in Ref. 31. Briefly, the reciprocal space dynamical matrix

$$\tilde{D}_{j\alpha j'\beta}(\mathbf{q}) = \sum_{l'} D_{j0\alpha,j'l'\beta} e^{i\mathbf{q}\cdot(\mathbf{R}_{j'l'}-\mathbf{R}_{j0})} \tag{17}$$

is calculated in a $4\times4\times4$ grid of $\mathbf{q}$ vectors. This grid is interpolated inside the Brillouin zone and the real-space force constants are obtained by means of an inverse Fourier transform. We find that such an interpolated grid gives well converged real-space force constants up to the fourth or fifth shell. The neglect of the shells beyond that introduces an error much smaller than other sources of error in the method. Finally, since the calculation of the DW factors uses clusters that typically include about 20 shells, the full force constant matrix for these clusters must be built by replicating the 3×3 $D_{jl\alpha,j'l'\beta}$ blocks obtained for each $jl,j'l'$ pair.

D. Lattice and force constants

The temperature-dependent lattice constant $a(T)$ is obtained by minimizing $F(a,T)$ in Eq. (9) with respect to a at a given temperature T. Within the electronic structure code ABINIT, the total VDOS $\rho_a(\omega)$ is calculated with histogram sampling in $\mathbf{q}$ space. However, we find it more convenient here to use a Lanczos algorithm in real space, similar to the approach used for the MSRD. This can be done by modifying the initial normalized displacement state $|0\rangle$ in Eq. (11) to that for a single atomic displacement, rather than the displacement along a given MS path. If more than one atom is present in the unit cell the contributions from each atom must be calculated and added. Similarly for anisotropic systems one must trace over three orthogonal initial displacements. Figure 2 shows a typical VDOS generated using the Lanczos algorithm. We find the free energies calculated with this approach deviate from the $\mathbf{q}$-space histogram method by less then 2 meV, i.e., to within 1%.

To minimize $F(a,T)$ efficiently we proceed as follows: First, the lattice constant is optimized with respect to the internal energy $E(a)$ and a potential energy surface (PES) for the cell expansion is built around the minimum. Second, the *ab initio* force constants are computed at each point of the PES to obtain the vibrational component of $F(a,T)$. Since this is the most time-consuming part of the calculation, we have taken advantage of the approximately linear behavior for small variations as illustrated in Fig. 1. Then, each element of the force constants matrix is interpolated according to

$$D_{jl\alpha,j'l'\beta} = A_{jl\alpha,j'l'\beta} + B_{jl\alpha,j'l'\beta}\Delta a \tag{18}$$

from just two *ab initio* force constant calculations with slightly different lattice parameters. This interpolation scheme allows us to reduce the computational cost of a typical calculation by a factor of 2/3, while introducing an error of less than 2% in the average frequencies. Once the values of $F(a,T)$ on the PES are obtained, we determine the minimum $a(T)$ by fitting $F(a,T)$ to a Morse potential

$$F(a,T) = D_0[e^{-2\beta(a-a(T))} - 2e^{-\beta(a-a(T))}]. \tag{19}$$

We have estimated that the numerical error in this minimization is of order 5×10^{-4} Å or less by fitting only the internal energy component $E(a)$ and comparing with the minima obtained using conjugate gradient optimization.

E. Computational details

All the ABINIT calculations reported here use Troullier-Martins scheme—Fritz-Haber-Institut pseudopotentials. We found that an $8\times8\times8$ Monkhorst-Pack k-point grid and an energy cutoff of 60 a.u. (12 a.u. for Ge) were sufficient to achieve convergence with respect to the DW factors. In all cases where the geometries were varied, an energy cutoff smearing of 5% was included to avoid problems induced by the change in the number of plane wave basis sets. For metallic systems, the occupation numbers were smeared with the Methfessel and Paxton[34] scheme with broadening parameter 0.025. Results are presented for LDA (Perdew-Wang

TABLE I. Born–von Karman parameters D_{ij}^{m} (N/m) from neutron scattering compared with *ab initio* calculations from this work.

	m	ij	LDA	GGA	hGGA	Exp.	
	110	xx	14.53	11.13	13.69	13.278	(Ref. 13)
Cu		zz	−3.17	−2.18	−3.46	−1.351	
49 K		xy	17.12	13.12	16.52	14.629	
	200	xx	1.07	0.85	1.31	−0.041	
		yy	−0.12	−0.11	−0.06	−0.198	
	110	xx	10.46	6.03	12.98	10.71(17)	(Ref. 29)
Ag		zz	−3.28	−1.65	−4.11	1.75(20)	
296 K		xy	12.48	7.27	15.94	12.32(32)	
	200	xx	1.06	0.70	1.34	0.06(29)	
		yy	−0.03	−0.08	−0.05	−0.23(19)	
	110	xx	14.22	9.17	17.97	16.43(09)	(Ref. 29)
Au		zz	−7.51	−5.31	−8.78	−6.54(10)	
295 K		xy	18.39	12.10	23.38	19.93(14)	
	200	xx	3.96	3.30	4.42	4.04(17)	
		yy	−0.33	−0.28	−0.25	−1.27(11)	
	110	xx	29.17	23.67	29.94	25.681(168)	(Ref. 30)
Pt		zz	−7.60	−6.67	−8.77	−7.703(251)	
90 K		xy	31.44	26.02	33.50	30.830(303)	
	200	xx	4.98	4.67	5.18	5.604(329)	
		yy	−1.56	−1.33	−1.28	−1.337(194)	

92[25]) and GGA (Perdew-Burke-Ernzerhof[26]) functionals, as well as for our mixed hGGA functional.

IV. RESULTS

A. Born–von Karman parameters

Phonon dispersion curves are often parametrized in terms of so-called Born–von Karman (BvK) coupling constants. These parameters are essentially the Cartesian elements of the real space dynamical matrix defined in Eq. (12). The main difference between the Born–von Karman parameters and force constants obtained within the quasiharmonic approximation is that the former are tabulated at specific temperatures while the temperature dependence of the quasiharmonic model arises implicitly from the dependence of the lattice parameters on thermal expansion. The dominant BvK coupling constants (up to the second neighbor) are presented in Table I.

We find that both the LDA with prescription I and the hGGA with prescription II generally give force constants that are within a few percent of experiment. Typically the LDA force constants with prescription I are slightly higher than those from the hGGA with prescription II. Also, note that the transverse components of the BvK parameters tend to be overestimated. We have also considered the pure PBE GGA functionals, but find that they produce force constants that are significantly weaker due to their larger equilibrium lattice constants (Fig. 1).

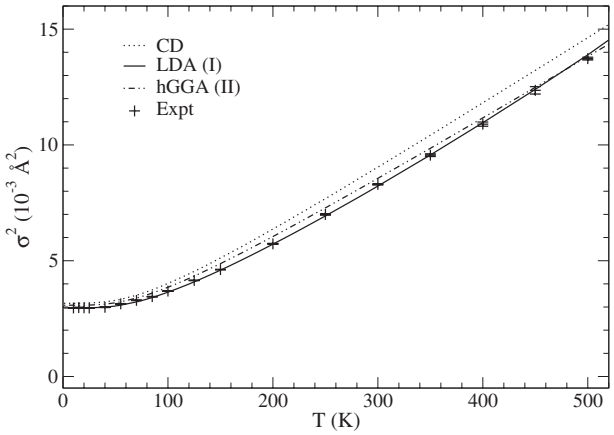

FIG. 3. Temperature dependence of the Debye-Waller factor for the nearest-neighbor single scattering path in Cu. The experimental difference values (Ref. 12) were shifted to match the LDA (I) results at 0 K.

B. Mean-square relative displacements

Calculations of the MSRD for the dominant first near neighbor path for fcc Cu are shown in Fig. 3, and detailed results for various scattering paths are presented in Table II. Both of our prescriptions I and II yield results in good agree-

TABLE II. Debye-Waller factors $\sigma_n^2(T)$ (in 10^{-3} Å^2) for the single scattering path to the nth shell of some fcc lattice metals. The experimental difference values were shifted to match the LDA (I) at 80 K and the experimental error (in parentheses) indicates the error in the least significant digits.

	n	CD	LDA(I)	GGA	hGGA(II)	Exp.	
Cu	1	6.11	5.48	6.79	5.80	5.57(05)	(Ref. 32)
190 K	2	7.49	7.49	9.20	8.01	7.4(3)	
	3	7.67	7.06	8.70	7.53	6.7(3)	
	4	7.76	7.02	8.68	7.48	7.0(5)	
Cu	1	9.04	8.22	10.45	8.56	7.99(16)	(Ref. 32)
300 K	2	11.16	11.44	14.31	12.03	11.2(5)	
	3	11.50	10.76	13.53	11.28	9.7(6)	
	4	11.66	10.70	13.49	11.20	11.4(10)	
Pt	1	3.55	3.23	3.91	3.23	3.22(05)	(Ref. 32)
190 K	2	4.38	4.64	5.57	4.78	4.7(3)	
	3	4.50	4.44	5.36	4.49	4.3(4)	
	4	4.56	4.60	5.55	4.66	4.5(4)	
Pt	1	5.41	4.98	6.08	4.90	4.83(05)	(Ref. 32)
300 K	2	6.69	7.23	8.71	7.34	6.8(5)	
	3	6.91	6.92	8.40	6.89	6.7(6)	
	4	7.01	7.17	8.71	7.16	7.0(6)	
Ag	1	3.78	3.69	4.89	3.38	3.9(3)	(Ref. 33)
80 K	2	4.56	4.97	6.57	4.60	5.4(5)	
	3	4.62	4.70	5.92	4.32	4.9(5)	
	4	4.64	4.67	6.22	4.28	5.5(5)	

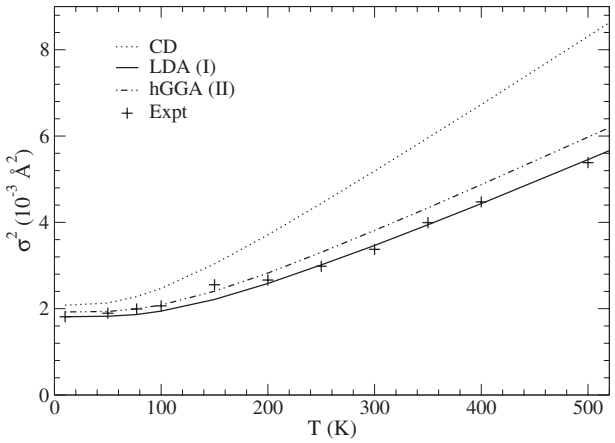

FIG. 4. Temperature dependence of the Debye-Waller factor for the nearest-neighbor single scattering path in Ge. The experimental difference values (Ref. 20) were shifted to match the LDA (I) results at 0 K.

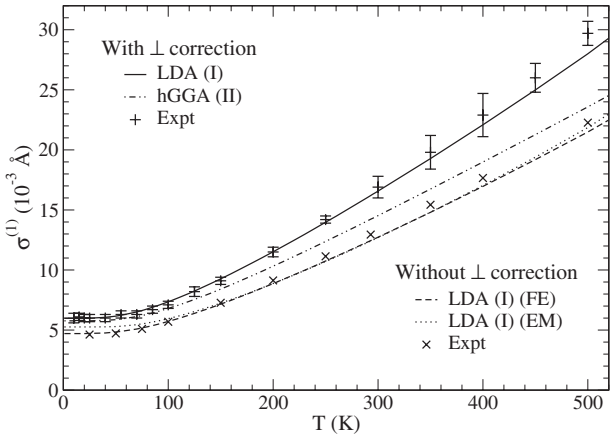

FIG. 5. Temperature dependence of the first cumulant for the nearest-neighbor single scattering path in Cu, with and without the perpendicular correction from Eq. (6), and obtained either from the minimization of the free energy (FE) or from the correlated Einstein model (EM). Both experimental difference values with (Ref. 12) and without (Ref. 22) the perpendicular motion correction were shifted to match the LDA (I) results at 0 K.

ment with experiment. For Cu even the correlated Debye model is quite accurate. Note also a slight deviation from linearity in temperature T due to the variation in the dynamical matrix with temperature is visible both in the experimental curve and in the calculation using prescription I.

Similarly, calculations of the MSRD for the first neighbor path in Ge are shown in Fig. 4, and detailed results for various scattering paths are given in Table III. Again, both of our prescriptions yield results in good agreement with experiment, with the LDA prescription being slightly better. For this case, however, the correlated Debye model with a single Debye temperature is significantly in error. This is not unexpected[1] since the projected density of modes $\rho(\omega)$ for diamond structures is anisotropic and dominated by optical modes for near-neighbor bonds. Tables II and III also include similar results for Ag, Pt, and GaAs.

C. Thermal expansion

The thermal expansion can now be calculated in two ways. First, by minimizing the free energy of the system using Eq. (9) one can obtain the overall thermal expansion, corresponding to the expansion of the lattice constant $a(T)$. For monoatomic systems the thermal expansion of any MS path is proportional to the lattice constant. More generally, the expansion is MS path dependent, and can be estimated using the correlated Einstein model of Sec. II C and the Appendix. From Eq. (16) and the Einstein model Grüneisen parameter $\gamma=-k_3R/k$, this model predicts that the first cumulant $\sigma^{(1)}$ has a temperature dependence proportional to the observed σ^2,

$$\sigma^{(1)} = \frac{3\gamma\eta}{R}\sigma^2. \tag{20}$$

As shown in Fig. 5 (dashed and dotted curves), this correlated Einstein model estimate for the thermal expansion agrees well with that obtained from minimizing the free energy of the system and with experimental crystallographic data.

TABLE III. Debye-Waller factors $\sigma_n^2(T)$ (in 10^{-3} Å^2) for the single scattering path for the nth shell of some diamond lattice semiconductors. The experimental difference values were shifted to match the LDA (I) at 80 K and the experimental error (in parentheses) indicates the error in the least significant digits.

	n	CD	LDA(I)	GGA	hGGA(II)	Exp.	
Ge	1	5.11	3.42	3.98	3.76	3.5(1)	(Ref. 32)
295 K	2	7.43	10.38	11.91	9.70	9.6(8)	
	3	7.64	13.09	15.03	11.84		
GaAs	1	5.17	3.97	4.59	3.86	4.2(1)	(Ref. 32)
295 K	2	7.75	12.70	14.28	12.01	11.7(14)	
(Ga edge)	3	7.69	14.91	16.29	14.01		
GaAs	1	5.15	3.96	4.59	3.86	4.2(1)	(Ref. 32)
295 K	2	7.20	10.80	11.69	10.19	9.6(11)	
(As edge)	3	7.68	14.83	16.66	14.00		

D. Perpendicular motion contributions

Figure 5 also shows the first cumulant for Cu obtained by adding the crystallographic component $\sigma^{(1)}=\bar{x}$ and the contribution due to perpendicular motion $\sigma_\perp^{(1)}$ from Eq. (6). As observed by Fornasini *et al.*,[12] the mean square perpendicular motion (MSPD) is correlated with σ^2, i.e., $\sigma_\perp^2=\gamma_\perp\sigma^2$, with an observed proportionality constant for Cu $\gamma_\perp \approx 2.5\pm0.3$.[35] The MSPD can be calculated using our Lanczos procedure with an appropriately modified seed state $|0\rangle$ for perpendicular vibrations. Thus the correlation between the MSPD and the MSRD reflects different projections of the same phonon spectra, and is generally expected to be temperature dependent. Indeed, our Lanczos procedure yields a ratio for $\gamma_\perp(T)$ that varies from 2.17 to 2.36 between 0 and 500 K, respectively, for Cu. Moreover, as shown in the Appendix, $\gamma_\perp(T)$ can be estimated for fcc structures using a correlated Einstein

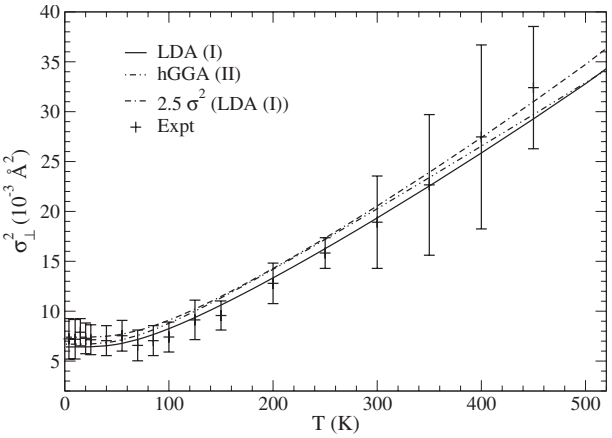

FIG. 6. Temperature dependence of the perpendicular component $\sigma_\perp^2$ of the Debye-Waller factor for the nearest-neighbor single scattering path in Cu. For comparison we also plot 2.5 σ^2 to show the correlation $\sigma_\perp^2 \approx \gamma_\perp \sigma^2$, together with the values extracted from experiment (Ref. 12).

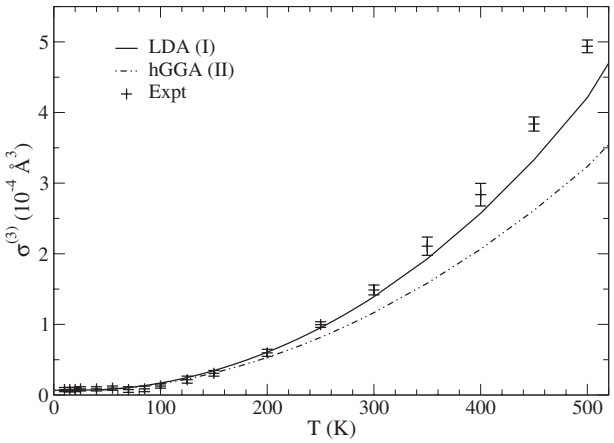

FIG. 7. Temperature dependence of the third cumulant for the nearest-neighbor single scattering path in Cu. The experimental difference values (Ref. 12) were shifted to match the LDA (I) results at 0 K.

model and gives 2.5 and $\sqrt{5} \approx 2.24$ at high and low temperatures, respectively. We also show for fcc structures that the correction due to perpendicular motion is smaller than the crystallographic contribution by a factor of $\gamma_\perp/6\gamma$, which for Cu is about 20%. To illustrate this correlation, Fig. 6 shows the perpendicular motion contribution $\sigma_\perp^2$ calculated both by the Lanczos procedure and with a constant correlation factor $\gamma_\perp = 2.5$.

We have carried out similar calculations of $\sigma_\perp^2$ for diamond lattices. Due to the strongly directional bonding in diamond structures, and non-negligible bond bending forces, the calculations are more complicated than for fcc materials. Our *ab initio* calculations using the LDA with prescription I yield a ratio $\gamma_\perp = 7.2(3.4)$ for 600 K (0 K), respectively, in reasonable agreement with experiment where $\gamma_\perp = 6.5 \pm 0.5(3.5 \pm 0.6)$ for the same temperatures.[35] In contrast a single near neighbor spring model, which is usually inadequate for the phonon spectra of diamond structures, gives a smaller high temperature value $\gamma_\perp = 3.5$.

E. Third cumulant

As for the first cumulant the third cumulant can be estimated from the correlated Einstein model and a generalized cumulant relation.[4,19] Again as in Eq. (16), it is desirable to express this relation in terms of the observed MSRD $\sigma^2 \approx \sigma^2(\omega_E, T)$ of Eq. (A5) rather than $\sigma^2(\bar{\omega}, T) = \eta\sigma^2(\omega_E, T)$ of the original cumulant relations, yielding (see Fig. 7)

$$\sigma^{(3)} = \eta\left[2 - \frac{4}{3}\left(\frac{\sigma_0^2}{\sigma^2}\right)^2\right]\sigma^{(1)}\sigma^2. \tag{21}$$

Note too that the moment ratio η gives another correction to the relation $\sigma^{(1)}\sigma^2/\sigma^{(3)} \approx 2$ derived for classical models[37] and single-spring models at high temperatures.

F. Crystallographic Debye-Waller factors

Finally, we present results for the x-ray and neutron crystallographic Debye Waller factors $W(T) = (1/2)k^2u^2(T)$, where the mean-square displacements $u^2(T) = \langle(\mathbf{u}\cdot\hat{\mathbf{R}})^2\rangle$ are given by Eq. (8), with $\rho_a(\omega)$ given by the total vibrational density of states per site, as calculated by our Lanczos algorithm with an appropriate seed state.[17] For this case good agreement is obtained for both of our DFT prescriptions at low temperature, although the errors become more significant at higher temperatures (Fig. 8). Also, we find that the convergence of the Lanczos algorithm is slower than for the path dependent Debye-Waller factors, requiring approximately 16 iterations to achieve convergence to 1%.

V. DISCUSSION AND CONCLUSIONS

Debye-Waller factors are essential to obtain a quantitative description of the amplitudes of various x-ray spectroscopies. These damping factors characterize the vibrational and structural disorder in a material, and thus may constitute a valuable probe of lattice dynamical structure in a system. Moreover, comparisons between calculated and mea-

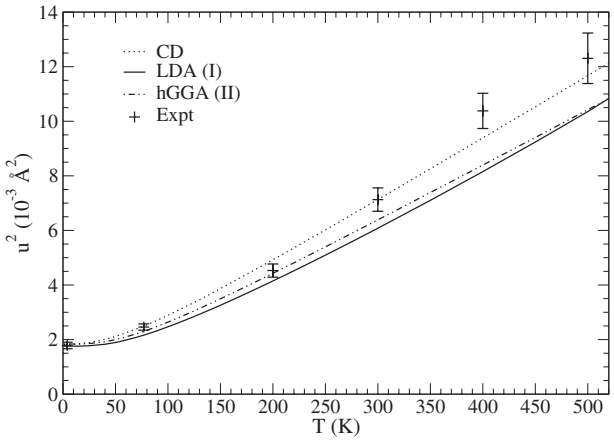

FIG. 8. Temperature dependence of the crystallographic Debye-Waller factor for the nearest-neighbor single scattering path in Cu, and compared to experimental values (Ref. 36).

sured DW factors can serve as a test of *ab initio* models of phonon structure. We have developed a first principles approach for calculations of these Debye-Waller factors, based on DFT calculations of the dynamical matrix and a Lanczos algorithm for the phonon spectra for a given system. We find that the results depend strongly on the choice of exchange-correlation potential in the DFT, however, we have developed two prescriptions that yield stable results: one of these is based on the LDA, and one is based on a modified GGA termed hGGA. Calculations for the crystalline systems presented here show that our LDA prescription yields good agreement with experiment for all quantities, typically within about ±10%. Second, if the lattice constant is known *a priori*, our hGGA prescription also provides an accurate procedure to estimate the MSRD.

Anharmonic corrections and estimates of the contribution from perpendicular vibrations are estimated using correlated Einstein models with calculated Einstein frequencies. For these anharmonic quantities, however, we have found that the comparative softness of the lattice dynamics with the GGA and hGGA functionals leads to results which are somewhat less accurate than those for the LDA. Finally we have also calculated the crystallographic Debye Waller factors. Our approach also yields good results for calculations of DW factors in anisotropic systems, as illustrated for Ge and GaAs. All of these results demonstrate that the prescriptions developed herein can yield quantitative estimates of Debye-Waller factors including anharmonic effects in various crystalline systems, and generally improve on phenomenological models. Thus these DW factors have the potential to yield significantly improved fits to XAS spectra. Extensions to molecular systems are in progress.

ACKNOWLEDGMENTS

We thank S. Baroni, K. Burke, A. Frenkel, X. Gonze, N. Van Hung, P. Fornasini, M. Newville, and J. Perdew for comments and suggestions. This work is supported in part by DOE Grant Nos. DE-FG03-97ER45623 (J.J.R.) and DE-FG02-04ER1599 (F.D.V.), and was facilitated by the DOE Computational Materials Science Network.

APPENDIX

In this Appendix, we briefly discuss the correlated Einstein model used in estimating anharmonic contributions to the DW factors. The model is illustrated with an application to the correlated Einstein model for calculating the MSRD σ^2 and the MSPD $\sigma_\perp^2 = \langle |\Delta \vec{u}_\perp|^2 \rangle$.

The construction of Einstein models is not unique in that different physical quantities reflect different averages over the VDOS. For example, the theoretical MSRD given by Eq. (8) reflects an average over a thermal weight factor which varies as $1/\omega^2$ at high temperatures. Thus the Einstein model parameters in our prescription are constructed to preserve the correct high temperature behavior of the MSRD,[1,3] $\sigma^2(T) \rightarrow \sigma^2(\omega_E, T) = k_B T/\mu\omega_E^2$. The first step in this construction is the calculation of $\bar{\omega}^2$ in Eq. (14) from the total potential energy for a net displacement x of a path along a particular seed displacement state $|0\rangle$. Next the spring constant is defined to give the correct high temperature MSRD

$$k_0 = \eta\mu\langle 0|\mathbf{D}|0\rangle = \eta\mu\bar{\omega}^2, \tag{A1}$$

where the factor $\eta = 1/\langle\omega^{-2}\rangle\bar{\omega}^2$, and $\langle\omega^{-2}\rangle$ is the inverse second moment of the projected VDOS. This inverse moment is obtained using the Lanczos algorithm of Eq. (11) for the VDOS. The cubic coupling k_3 is then defined to be consistent with the variation in k given by the Grüneisen parameter

$$\gamma = -\frac{d\ln\bar{\omega}}{d\ln R^3} = -\frac{k_3 R}{k}. \tag{A2}$$

Consequently k_3 must also have a factor η to preserve the observed lattice expansion

$$k_3 = \frac{\eta}{6}\frac{d}{dR}\langle 0|\mathbf{D}(R)|0\rangle. \tag{A3}$$

Then the Einstein frequency ω_E in the quasi-harmonic approximation is obtained from the relation[18]

$$k = k_0 + 6k_3\bar{x} = \mu\omega_E^2. \tag{A4}$$

where μ is the reduced mass. For Cu the Lanczos algorithm with the LDA (I) prescription for the dynamical matrix then yields $\eta = 0.73$, $k_0 = 54.7$ N/m, $k_3 = -48.4$ N/mÅ, and $k = 51.1$ N/m. With these definitions our correlated Einstein model for $\sigma^2(T)$ is

$$\sigma^2(\omega_E, T) = \sigma_0^2 \coth\left(\frac{\beta\hbar\omega_E}{2}\right), \tag{A5}$$

where the zero-point value $\sigma_0^2 = \sigma^2(0) = \hbar\omega_E/2k$.

Note, however, that the original relations between the cumulants[19] were derived for single-spring models with Einstein frequency given by $\bar{\omega}$ in Eq. (14). Thus to obtain the modified relations with the factors of η in Eqs. (16) and (21), one must simply replace $\sigma^2(\bar{\omega}, T) \rightarrow \eta\sigma^2(\omega_E, T)$. No additional scaling factor is needed for $\sigma^{(1)}$ since the free energy Eq. (9) is only weakly (logarithmically) sensitive to the phonon frequency distribution, and hence can be modeled by an Einstein model with frequency $\bar{\omega}$. Although our derivation is based on the high temperature behavior, the validity of these relations at low T is corroborated by experiment (Figs. 5 and 7). Thus given the MSRD σ^2 and the relations between the cumulants discussed above, one can obtain MS path-dependent estimates for $\sigma^{(1)}$ and $\sigma^{(3)}$.

As a second example of Einstein model, we construct a model for monoatomic fcc Cu starting from an anharmonic pair potential.[4,19] That is, we assume that the lattice dynamics can be described by a pair potential V_0 between near-neighbor atoms of the form

$$V_0(x) \cong \frac{1}{2}k^0 x^2 + k_3^0 x^3. \tag{A6}$$

Here x is the net displacement x along the bond direction, with positive displacements referring to expansion and negative to compression.

To carry out this construction, first consider the potential energy $V_\parallel(x)$ for vibrational displacement x along the bond

$(0R)$ between lattice points (0,0,0) and $\vec{R}=R(0,1,1)/\sqrt{2}$. The net anharmonic potential $V_{\parallel}(x)$ is then given by Eq. (15) with a displacement state $x|0\rangle$ defined by $\vec{u}_0=(x/2)(0,1,1)/\sqrt{2}$, and $\vec{u}_R=(-x/2)(0,1,1)/\sqrt{2}$. Then constructing the dynamical matrix using Eq. (A6) with small displacements, we find a net spring constant $k_0=\eta\langle 0|D|0\rangle=(5\eta/2)k^0$, in agreement with Ref. 4. This result can alternatively be obtained by summing the 23 pair potentials between the shared bond $(0R)$, the 11 nearest-neighbor bonds to the origin and the 11 other nearest-neighbor bonds to R, giving $V_{\parallel}(x)=V_0(x)+2V_0(-x/2)+8V_0(x/4)+8V_0(-x/4)+4V_0(0)$. Similarly we find that the anharmonic coupling [cf. Eq. (A3)] is $k_3=(3\eta/4)k_3^0$, so that

$$V_{\parallel}(x)=\frac{1}{2}\left(\frac{5\eta}{2}k^0\right)x^2+\left(\frac{3\eta}{4}k_3^0\right)x^3, \tag{A7}$$

where we have again included a factor η so that the Einstein model for σ^2 agrees with the expression from the inverse second moment of the VDOS.

In a similar way, we can develop a correlated Einstein model to describe the perpendicular vibrations. For this case we consider a vibrational displacement $\Delta\vec{u}_{\perp}$ of length $y=|\Delta\vec{u}_{\perp}|$ perpendicular to the bond between $(0,R)$. Thus we set $\vec{u}_0=(y/2)(0,1,-1)/\sqrt{2}$ and $\vec{u}_R=(-y/2)(0,1,-1)/\sqrt{2}$, where R is the nearest-neighbor distance. The net potential $V_{\perp}(y)$ is again obtained by summing the 23 pair potentials between the shared bond $(0R)$, the 11 nearest-neighbor bonds to the origin and 11 others to R, similar to the calculation above for vibrations along the bond. For this case, two bonds are stretched by $y/2$, two contracted by $y/2$, three unchanged, eight stretched by $y/4$, and eight contracted by $y/4$, yielding a net sum $V_{\perp}(y)=2V_0(y/2)+2V_0(-y/2)+8V_0(y/4)+8V_0(-y/4)+3V_0(0)$, and hence

$$V_{\perp}(y)=\frac{1}{2}(2\eta k^0)y^2. \tag{A8}$$

Note that by symmetry, the net cubic anharmonic contribution vanishes. Thus the effective spring constant for the MSPD is $k=2\eta k^0$ and predicted to be insensitive to thermal expansion. The correlated Einstein model $V_{\perp}(z)$ is clearly the same for the MSPD along the z axis.

With these results we can show that the MSPD for the first neighbor path in fcc materials $\sigma_{\perp}^2$ is correlated with $\sigma^2=\langle|\Delta\vec{u}_{\parallel}|^2\rangle$. Both the MSPD and MSRD in the Einstein model are given by Eq. (A5), with their respective Einstein frequencies $\omega_E=(k/\mu)^{1/2}$. For the total contribution from perpendicular vibrations, one has to multiply by two to get the net $\sigma_{\perp}^2$ from both independent axes. At high temperatures, we obtain the MSPD $\sigma_{\perp}^2=2k_BT/2\eta k^0$. This is higher than the MSRD $\sigma^2=(2/5)k_BT/\eta k^0$ by a factor of $\gamma_{\perp}=5/2$. The model also predicts a weakly temperature-dependent ratio

$$\gamma_{\perp}(T)=\frac{\sigma_{\perp}^2(T)}{\sigma^2(T)}=2\frac{\omega_E\coth(\beta\hbar\omega_E^{\perp}/2)}{\omega_E^{\perp}\coth(\beta\hbar\omega_E/2)}, \tag{A9}$$

which varies between $\sqrt{5}=2.236$ and 2.5 with increasing temperature. Thus the ratio $\gamma_{\perp}$ obtained with the correlated Einstein model for the fcc lattice depends only on geometry and describes the anisotropy of the vibrational ellipsoid in monoatomic fcc structures reasonably well. Because of this relation the perpendicular contribution to the first cumulant can be related to the lattice expansion, i.e., from Eqs. (6) and (20),

$$\frac{\sigma_{\perp}^{(1)}}{\sigma^{(1)}}=\frac{\gamma_{\perp}}{6\eta\gamma}. \tag{A10}$$

For fcc Cu this result gives a correction to the first cumulant $\sigma^{(1)}$ of about 25%. Such a shift is comparable to the differences in the thermal expansion with and without the perpendicular motion term as observed in Fig. 5. Thus for the dominant near neighbor bonds, the correlated Einstein model predicts a comparatively small but non-negligible contribution from perpendicular vibrations to EXAFS distance determinations.

[1] E. D. Crozier, J. J. Rehr, and R. Ingalls, in *X-Ray Absorption: Principles, Applications, Techniques of EXAFS, SEXAFS, and XANES*, edited by D. C. Koningsberger and R. Prins (Wiley, New York, 1988), p. 375.

[2] V. V. Shmidt, Bull. Acad. Sci. USSR, Phys. Ser. (Engl. Transl.) **27**, 392 (1963).

[3] E. Sevillano, H. Meuth, and J. J. Rehr, Phys. Rev. B **20**, 4908 (1979).

[4] N. Van Hung and J. J. Rehr, Phys. Rev. B **56**, 43 (1997).

[5] A. Poiarkova and J. J. Rehr, J. Synchrotron Radiat. **8**, 313 (2001).

[6] H. J. Krappe and H. H. Rossner, Phys. Rev. B **66**, 184303 (2002).

[7] S. Baroni, S. de Gironcoli, A. Dal Corso, and P. Giannozzi, Rev. Mod. Phys. **73**, 515 (2001).

[8] C. Lee and X. Gonze, Phys. Rev. B **51**, 8610 (1995).

[9] G.-M. Rignanese, J.-P. Michenaud, and X. Gonze, Phys. Rev. B **53**, 4488 (1996).

[10] S. Narasimhan and S. de Gironcoli, Phys. Rev. B **65**, 064302 (2002).

[11] R. Kubo, J. Phys. Soc. Jpn. **17**, 1100 (1962).

[12] P. Fornasini, S. a Beccara, G. Dalba, R. Grisenti, A. Sanson, M. Vaccari, and F. Rocca, Phys. Rev. B **70**, 174301 (2004).

[13] R. M. Nicklow, G. Gilat, H. G. Smith, L. J. Raubenheimer, and M. K. Wilkinson, Phys. Rev. **164**, 922 (1967).

[14] A. V. Poiarkova and J. J. Rehr, Phys. Rev. B **59**, 948 (1999).

[15] N. Dimakis and G. Bunker, Phys. Rev. B **58**, 2467 (1998).

[16] P. Deuflhard and A. Hohmann, *Numerical Analysis* (de Gruyter, Berlin, 1995).

[17] H. H. Rossner, D. Schmitz, P. Imperia, H. J. Krappe, and J. J. Rehr, Phys. Rev. B **74**, 134107 (2006).

[18] A. A. Maradudin and P. A. Flinn, Phys. Rev. **129**, 2529 (1963).

[19] A. I. Frenkel and J. J. Rehr, Phys. Rev. B **48**, 585 (1993).

[20] G. Dalba, P. Fornasini, R. Grisenti, and J. Purans, Phys. Rev. Lett.

82, 4240 (1999).
[21] J. G. Collins, Philos. Mag. **8**, 323 (1963).
[22] *American Institute of Physics Handbook* (McGraw-Hill, New York, 1972).
[23] J. Tao, J. P. Perdew, V. N. Staroverov, and G. E. Scuseria, Phys. Rev. Lett. **91**, 146401 (2003).
[24] V. N. Staroverov, G. E. Scuseria, J. Tao, and J. P. Perdew, Phys. Rev. B **69**, 075102 (2004).
[25] J. P. Perdew and Y. Wang, Phys. Rev. B **45**, 13244 (1992).
[26] J. P. Perdew, K. Burke, and M. Ernzerhof, Phys. Rev. Lett. **77**, 3865 (1996).
[27] J. P. Perdew (private communication).
[28] X. Gonze *et al.*, Comput. Mater. Sci. **25**, 478 (2002).
[29] W. A. Kamitakahara and B. N. Brockhouse, Phys. Lett. A **29**, 639 (1969).
[30] D. H. Dutton, B. N. Brockhouse, and A. P. Miiller, Can. J. Phys. **50**, 2915 (1972).
[31] X. Gonze and C. Lee, Phys. Rev. B **55**, 10355 (1997).
[32] E. A. Stern, B. A. Bunker, and S. M. Heald, Phys. Rev. B **21**, 5521 (1980).
[33] M. Newville, Ph.D. thesis, University of Washington, Seattle, 1995.
[34] M. Methfessel and A. T. Paxton, Phys. Rev. B **40**, 3616 (1989).
[35] P. Fornasini (unpublished).
[36] P. A. Flinn, G. M. McManus, and J. A. Rayne, Phys. Rev. **123**, 809 (1961).
[37] E. A. Stern, P. Līvņš, and Z. Zhang, Phys. Rev. B **43**, 8850 (1991).